

Original Article

Power Control System Fabrication for Sample Holder with Heating Hot Filament

Leonardo Carlos Afonso¹, José Roberto R. Bortoleto¹, Péricles Lopes Sant'Ana¹

¹State University of São Paulo – Technological Plasmas Technology, Alto da Boa Vista, Sorocaba, SP, Brasil.

drsantanapl@gmail.com

Received: 12 January 2023; Revised: 10 February 2023; Accepted: 25 February 2023; Published: 15 March 2023;

Abstract - In this article, we introduce the fabrication of a phase-angle power controller module and its coupling of a hot filament for heating a sample holder in low-pressure plasma systems. The sample holder was adapted to a vacuum system for the growth of oxide films by the PECVD (*Plasma Enhanced Chemical Vapor Deposition*) technique in order to control the temperature of the substrate during the film deposition. Then, the power circuit was based on the TRIACs circuit, while the temperature was measured using a thermocouple coupled to the front of the sample holder. A microcontroller from Microchip's PIC 18F family was used to control the module. Finally, the PID control logic was developed in C language. Results showed that the heating of the sample holder reached over 70 °C for over 1200 s, in a growing and non-linear fit. Diverse surface properties of these films found many applications in nanotechnology, and the temperature during the film growth is a key parameter for film properties, including the nucleation in the first stages, surface morphology, wettability, transmittance and absorbance at the visible range, electrical surface properties and others.

Keywords - PID control, Phase angle triggering, PECVD, Temperature.

1. Introduction

In the last years, great scientific and technological interest in the development of new materials and structures has been observed at the nanoscale (i.e. graphene and carbon nanotubes [1] and semiconductor quantum dots [2-3]. For semiconductors studies, great efforts have been made to construct nanostructures, both self-formed and constructed by lithography techniques [5], to characterize their physical properties. These semiconductor nanostructures are potential for application in lasers technology, and solid-state LED's with high efficiency and new devices were constructed, such as the single electron transistor, optical memories and even quantum computers [6]. For polymeric materials, plasma deposition techniques have been used for mechanical, tribological and chemical properties improvement, mainly on the surface, when the dimensions are reduced [7]. Aside from this, the manufacture of transistors, photovoltaic and optical devices was possible using conductive polymers [8], chemical sensors [9], and others.

In the area of surface treatment and thin films, the application of electrical discharge plasmas in low-pressure regimes has been highlighted as performing a series of peculiar characteristics: high speed when scaled up, low cost and absence of harmful residue production. In addition, it also allows replicated control of the modifications, making the adjustment of properties that are desired to obtain. Hence, the PECVD technique [10,11] allows for obtaining thin films with a wide range of properties by controlling the process parameters, as seen for insulating/conductive layers growth (with controlled thickness) besides its use for the manufacture of electronic



devices [12], transparent films suitable for optical windows, anti-reflective layers, coatings for lenses and sports glasses [13], biocompatible films [13] and for other applications [14] such to obtain hydrophobic materials [15] suitable for food packaging and sensor manufacturing design.

2. Materials and Methods

2.1. Thin Film Deposition

The plasma deposition system used consists of a stainless-steel vacuum chamber with two internal circular parallel electrodes. Then, 6 glass substrates were placed on the stainless-steel electrode after ultrasonicated for three consecutive baths of 20 min. Each, with pure water, industrial detergent and isopropyl alcohol, respectively. Then, the system was evacuated by a rotary pump ($18 \text{ m}^3/\text{h}$) down to 10^{-1} Pa . Needle valves were employed to control the gas feeding and a Pirani pressure sensor to monitor the chamber pressure. Glass samples were exposed directly to the plasma environment established by the application of Radiofrequency Power (13.56 MHz) at 100 W to an atmosphere composed of O₂ and Zinc precursor via Erlenmeyer fixed to the reactor. Oxygen flow was fixed to 10 sccm, keeping the total pressure constant at 6.66 Pa (50 mtorr). The treatment time was 30 min. Fig. 1 shows the scheme of PECVD applied to a deposition system installed in the Technological Plasmas Laboratory in UNESP for ZnO thin film deposition. At the same time, the sample holder was heated to until 70 °C.

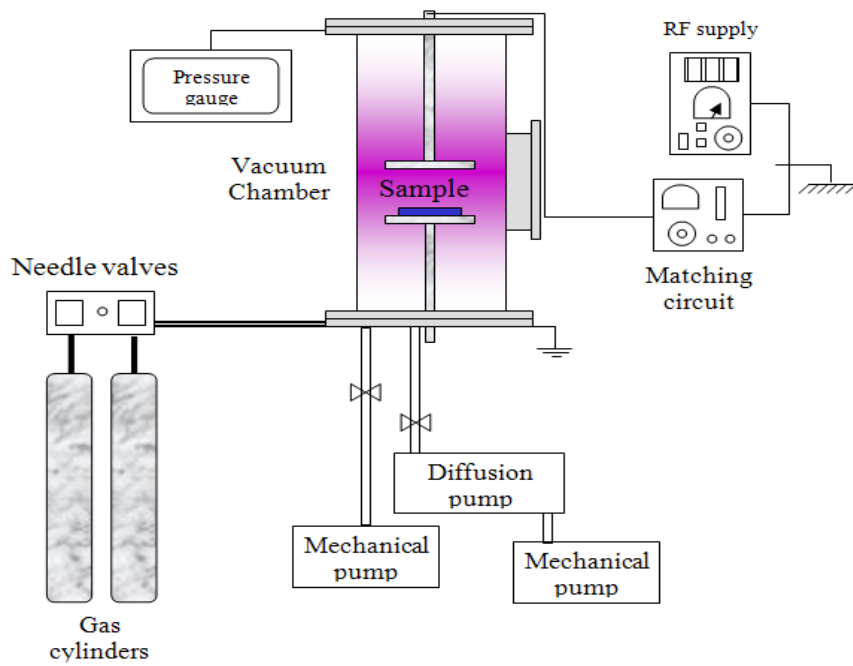


Fig. 1 Scheme of PECVD configuration employed for thin film deposition or surface treatment

Concerning the experimental design, Fig. 1 shows a schematic of the PECVD process; when organic or organometallic vapors, and their mixtures with reactive and noble gases, are introduced into the electrical discharge region, hence, a thin film with well-defined characteristics usually grows on the solid surfaces (samples). These thin films can be either organic or inorganic, depending on the chemical composition of the plasma. On the other hand, starting from the same mixture, polymeric films (low density and soft amorphous) can be grown. [13], hydrogenated amorphous carbons (moderately dense and as hard as 40 GPa) [16]] or even graphitic carbon (with a highly ordered structure, a high proportion of sp₂ states and low hardness) [17]. Such results depend on the different degrees of interaction between the plasma and the surface [11] and may be

controlled by the electrical discharge regime, its electrical power and the temperature of the substrate during film formation [10]. For this and other reasons, it is necessary to heat the sample holder during plasma processing, which influences the grain formation mechanism and initial morphology, mainly in the first stages of nucleation.

2.2. Methods and Tools to Fabricate the Circuits and the Power Controller

Any type of control needs a plant (sample holder, resistance and PECVD reactor), sensor (type K thermocouple) and actuator (electrical resistance). Consequently, this work is divided into three parts: data acquisition, actuation, and control systems. The temperature of the sample holder was controlled by firing a TRIAC, which changes the amount of energy that the electrical resistance dissipates when changed. This amount of energy varies according to the difference between the value of the setpoint (expected temperature) and the measured temperature. A PID control was implemented to handle this error and drive the system to the expected temperature. The equation that fit the sample holder system together with the filament hot water was modeled using MATLAB software. In particular, a curve experiment was raised using the temperature points as a function of time (sampled through a microcontroller). So, knowing the behaviour approximated to the thermal plant, a theoretical curve was fitted, and the equation was found. The materials and software used in this project were: a PIC18F4550 microcontroller; Type K thermocouple; Printed circuit board; Resistors and capacitors; MAX6675, Microtubular resistance; parallel circular sample holder; a Matrix keyboard; a MikroC compilation software 8.2; a Proteus simulation software 7.2; and a MATLAB program.

3. Theoretical Review: Electronic Circuits for Instrumentation Devices

3.1. Synchrony Circuit with the Network

In this work, an electronic circuit that synchronized the microcontroller with the network was designed and characterized. This was necessary for the microcontroller to recognize where the sine wave from the network starts, thus triggering the TRIAC according to the PID control.

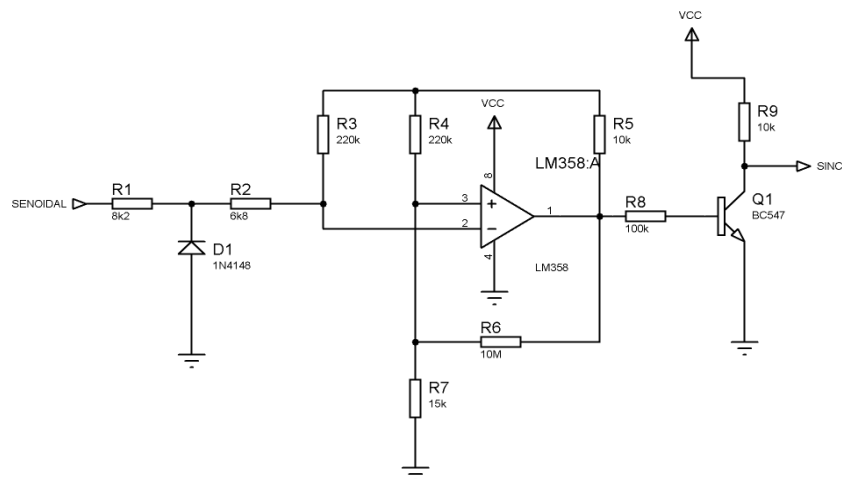


Fig. 2 Schematic of a zero cruiser using Op-amp

In this circuit, the LM358 Op-amp is in the voltage comparator configuration. When the mains voltage (which was lowered using a transformer to 6Vrms) reaches values above zero, it generates a positive square wave of 4V. In order to adapt to the values of the microcontroller (5V), a transistor was implemented as a switch, thus obtaining the following voltage form for the sync point:

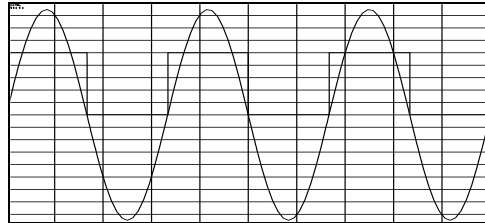


Fig. 3 Square wave generated by the synchronism circuit in relation to the sine wave after passing through a 6+6V transformer

3.2. Power Controller Circuit

This circuit can control the power delivered to the resistor by changing a TRIAC's firing angle, so the voltage's rms value changes from a maximum value (127V) to a minimum value (0V).

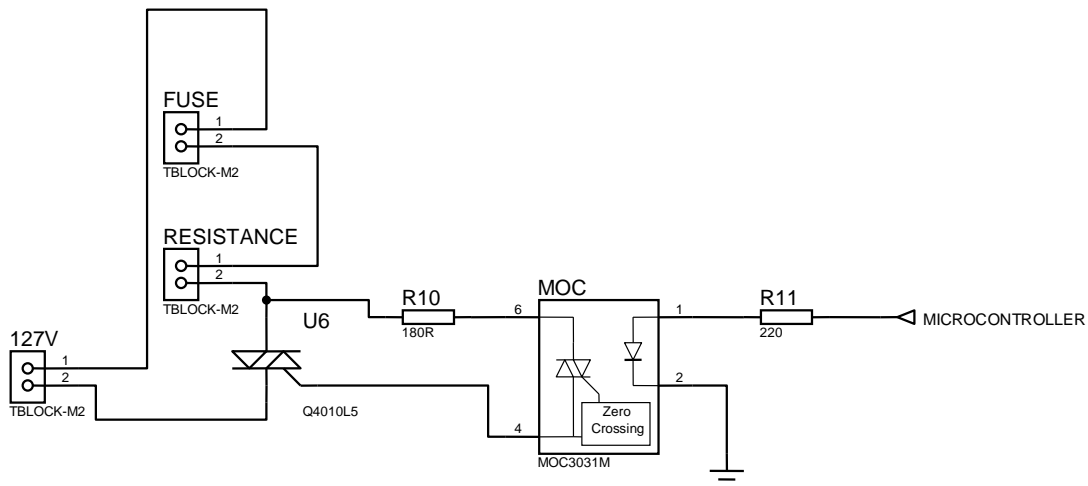


Fig. 4 Discrete TRIAC driver schematic that can supply up to 10A rms to the resistive load

A phototriac was used in the process to decouple the control circuit from the source that generates the power for the resistance, thus avoiding electrical currents and voltages that could damage the control circuit.

3.3. Temperature Meter Circuit

Aiming to measure the temperature in the sample holder, a circuit was designed that, from a type K thermocouple, would show the temperature on an LCD display and in a program on the PC. For this, Maxim's MAX6675 integrated was used, which performs all the amplification and digitalization of the thermocouple signal and sends it serially through the SPI protocol.

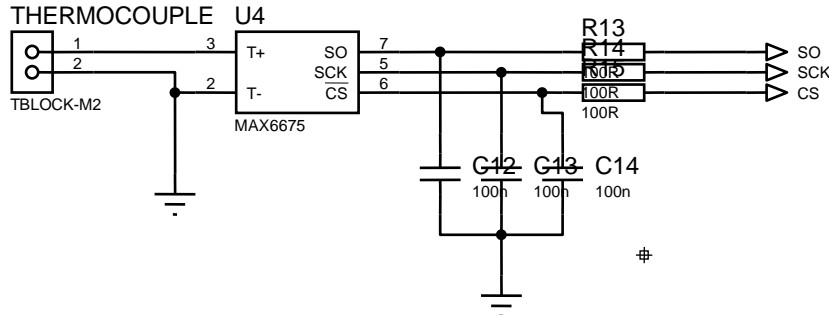


Fig. 5 Schematic of the MAX6675 integrator that obtains the analog values from the K-type thermocouple and transforms it into digital

3.4. USB Interface

Realizing that the circuit may be activated through a program in a future application, a USB interface was designed using the PIC18F4550, a connector and capacitors.

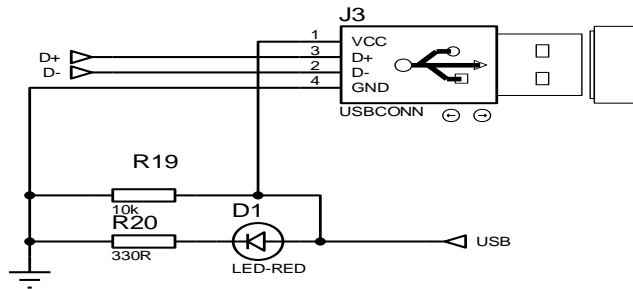
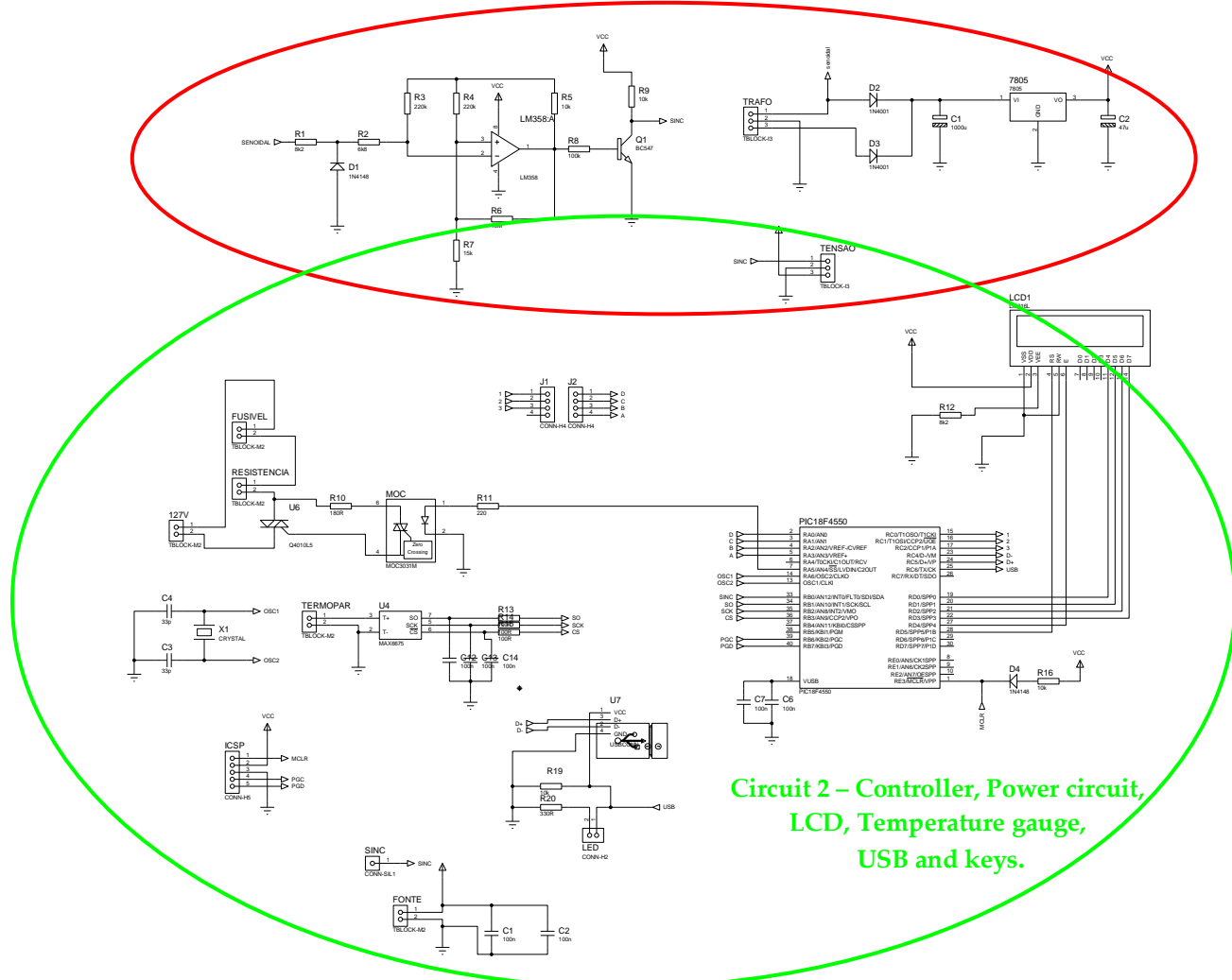


Fig. 6 USB connector connection diagram

4. Results

It was possible to obtain the schematic integrated circuit by putting together all the circuits presented above and the regulated voltage source.

Circuit 1 – regulated Source (+5V) and synchrony circuit



4.1. Power Control System

The system generated using the power control circuit can be observed via the scheme from Fig. 8.

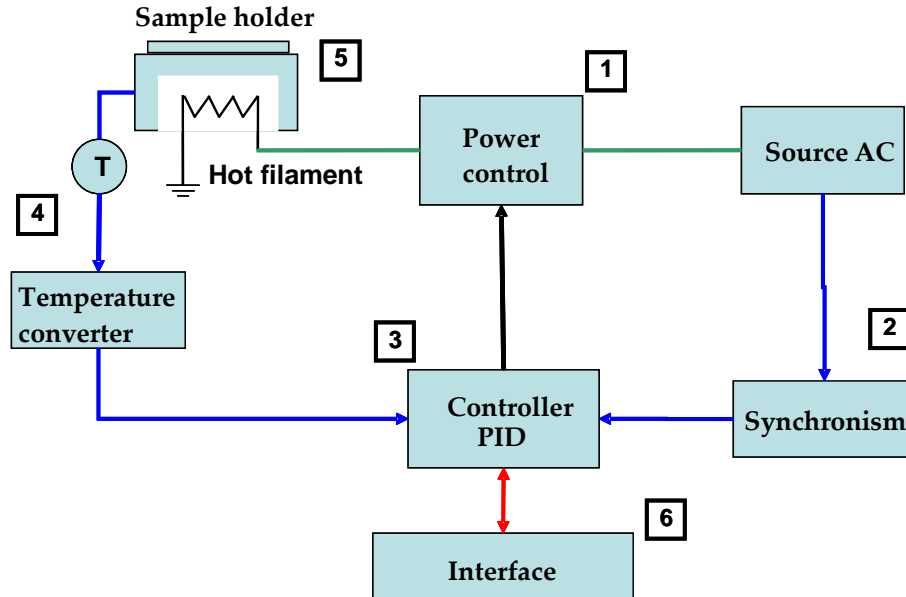


Fig.8 Scheme of the electrical circuit exhibits the main integrated parts of the power control while the numbers indicate the project development sequences

4.2. Programs for the Power Controller, Construction of the PID Logic for the System and Preliminary Control Tests

4.2.1. Printed Circuits

Using PROTEUS ARES 7.2 program, the printed circuit for the boards was designed. It was separated into a source+synchronism circuit and a power control circuit+temperature meter+LCD+USB. So, we have the PCB board for both (circuits 1 and 2 from Fig. 7) as seen as supplementary figures. Once the schedule was finished, these circuits were produced on printed circuit boards using conventional methods. Fig. 9 shows the photo of circuit boards 1 and 2.



Fig. 9 Photograph showing circuit boards 1 and 2 being used in a test to control the power in a tungsten incandescent lamp, as identified by "circuito 1" and "circuito 2"

4.2.2. Programs for the Power Controller

As the communication of the IC chosen for the interpretation of the generated voltages of the thermocouple is SPI, a microcontroller was used to generate a program that interpreted these data, showing the user the reactor's temperature. The microcontroller chosen was the PIC18F4550 which has low cost, good performance for the C language and comes with a USB peripheral that makes it suitable for this work.

4.2.3. Microcontroller Initialization

For the correct functioning of the microcontroller, it is first necessary to initialize it, where it is defined how its registers will work. Thus, Timer1 was configured to control the firing angle and the external interruption that tells when the sine wave of the network starts its cycle. As the only input of the system, so far, is the synchronism, only pin 0 of port B was put as an input.

4.2.4. Acquisition of Temperature Data

First, a program was made to analyze the data coming from the MAX6675 CI. Your data uses a serial protocol SPI; knowing this, a program was created that emulates this protocol. This protocol has clock, data, and chip select pins. The data, acquisition time and clock frequency were found in the component's datasheet. The acquisition time is 220ms, and the maximum clock frequency is 4.3MHz. Fig. 10 represents the signal logic for the MAX6675 integrated operation. Not all the bits in this Word represent the temperature, but some are discarded, such as the stop and start bits typical of serial communication. The representative data are shown in figure 11. The following program is for reading the data, so when reading is requested, it places the component's select chip at a low logic level; after that, it generates a square wave on the receiving clock pin 16 bits on the data pin and stores them in the temp variable.

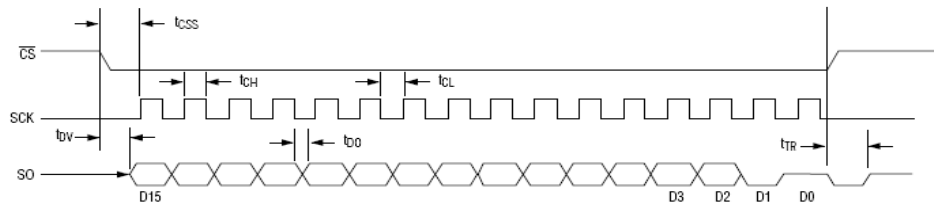


Fig. 10 Signals for the operation of the integrated MAX6675, chip select (CS), SCK (Serial clock), and SO (Serial Output)

BIT	DUMMY SIGN BIT	12-BIT TEMPERATURE READING												THERMOCOUPLE INPUT	DEVICE ID	STATE	
		15	14	13	12	11	10	9	8	7	6	5	4	3			
Bit	15	14	13	12	11	10	9	8	7	6	5	4	3	2	1	0	
	0	MSB												LSB		0	Three-state

Fig. 11 Signal received by the MAX6675 microcontroller, from bits 3 to 14, there is the thermocouple temperature, where bit 3 is the least significant bit of temperature and bit 14 is the most significant. Of these 12 bits, the two least significant give a precision of 0.25°, and the 10 most significant ones show the temperature from 0 to 1024°C. Bit 2 indicates the presence or absence of the thermocouple

With these subroutines created, a main program was made to read the temperature and show it on an LCD display. In this routine, every 450ms, a request is made for the Max6675 to send the data, so the temperature data is stored in the variable t. If the variable sterm is in logic level 0, it means that the thermocouple is present, and then the variable t is shown in the LCD; if the sterm variable is 1, it means no thermocouple.

To test the temperature reading, the temperature value of a hot plate was measured and compared with the value indicated by a commercial thermometer type PT100. The data obtained in the range from 0 to 150°C are shown in table 2. It can be noted that the percentage difference for temperatures above 50°C (range of interest in

PECVD) is less than 2.0%. For initial tests, the sample holder in a plasma environment (pressures below 1 torr) will be loosing thermal energy mainly through thermal radiation. Remembering Planck's radiation law it has:

$$\frac{dE}{dt} = \sigma AT^4 = P_R \quad (1)$$

$$5.670 10^{-8} \frac{W}{m^2 K}$$

where is the Stefan-Boltzmann constant and is equal to

In this case, considering the construction of a cylindrical sample holder with a diameter d=0.10 m, the

$$A = \pi \frac{d^2}{2} \approx 0,016 \text{ m}^2.$$

effective radiation area can be

Therefore, for a power of 1100 W, the equilibrium temperature would be equal to 1049.35 K, that is, approximately 776° C. This guarantees that desirable temperatures for the growth of oxide films of up to 500 °C can be reached with the module of power to be designed.

Table 2. Temperature values measured with the circuit and thermocouple and a commercial thermometer in the range until 150° C

Attempt	Thermocouple (°C)	Thermometer (°C)	Percent Difference (%)
1	24	27	-11.0
2	34	36	-5.0
3	86	88	-2.0
4	109	111	-1.8
5	113	114	-0.9
6	119	120	-0.8
7	136	135	0.7
8	141	140	0.7

4.2.5. Trigger Angle Control

To control the power dissipated in the hot filament, a TRIAC (triode alternating current) thyristor is used [18-20]. Thyristors are semiconductor devices whose electrical conduction condition is controlled by applying a certain signal to the control electrode (gate). The conduction, once started, is maintained even in the absence of the command signal until the current passing through it drops below a certain value, called the operating current. In the case of the TRIAC, it conducts electric current in both directions when a trigger pulse (positive or negative) is injected into its gate, as seen in Fig. 12 for a load voltage as a function of time.

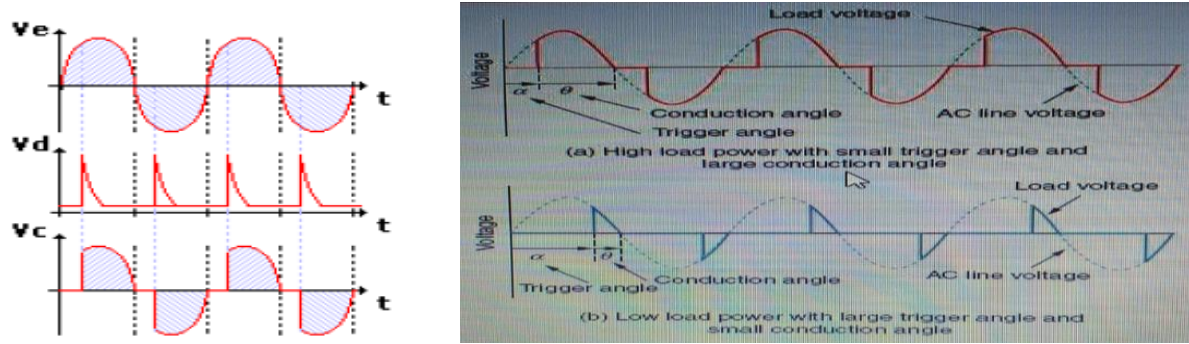


Fig. 12 Phase angle schemes when a Voltage is applied as a function of time. TRIAC tripping usually occurs by a voltage present in the input voltage waveform at a certain angle predetermined by the designer. For the maintenance of the TRIAC, a minimum current is required; after the TRIAC is triggered, it continues to conduct until its current becomes lower than the maintenance current, causing its shutdown. V_e , V_d , and V_c as a function of time represent, respectively: the input AC, trigger pulse (clock) and voltage on the filament.
Usually, the voltage forms are used for an AC load with phase control

The program made in the microcontroller reaches into interruption when the synchronism circuit informs that this is the beginning of the wave, from which TIMER1 is activated, which in this case is set to fire every millisecond. If the trigger angle is less than 180°, TIMER1 counts back to trigger the TRIAC at 180, leaving the conduction complete until a new wave.

It was certified that the square wave generated by the synchronization circuit oscillates when a transient (Debounce) occurs, so in the interrupt routine, a flag was placed that indicates the first rising edge caused by the zero crosses and interrupts the interruptions until the circuit counts the trigger time. Then, it can set any trigger angle and continue reading the temperature since the microcontroller is not “stopped” to intervene in the wave. Then, Fig. 13 shows the Photos fitting the power circuit driving voltage across the load at varying times: (a)0 ms; (b)4ms; (c)8,3ms; (d)15ms.

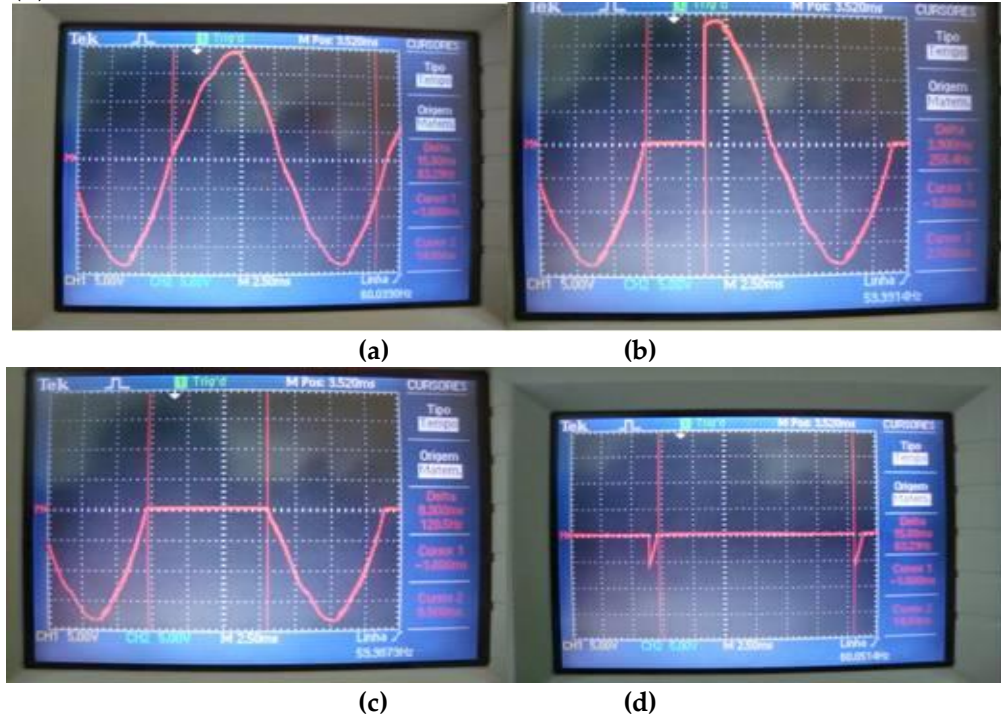


Fig. 13 Photographs showing the power circuit driving voltage across the load at varying times: (a)0 ms; (b)4ms; (c)8,3ms; (d)15ms

4.2.6. Construction of PID Logic For The System

The combination of proportional, integral and derivative actions to generate a single control signal gives rise to what we call a proportional-integral-derivative controller or simply PID. The objective is to take advantage of the particular characteristics of each of these actions to obtain a significant improvement in the transient and steady-state behavior of the controlled system. Therefore, the PID control proves to be very robust and is the most used in practical realizations.

In order to obtain the best result from the controller, MATLAB software was used in this project, which has a range of tools that help in the production of controllers and provide a simulation close to reality. First, all signals (Setpoint and sensor) must be treated to be in a mode the microcontroller can analyze. Therefore, the thermocouple signal was amplified and passed through a digital analog circuit (MAX6675) and the keyboard signal was treated and remained in the same form as the thermocouple signal.

The microcontroller output must take into account the nonlinearity of the trigger angle versus rms voltage relationship, so the system must know the digital-trigger angle and trigger angle-rms voltage relationship, in which the scheme can be designed as assembled in a flowchart for better understanding. Hence, the analyses of the signals were made, and their relationships were raised.

4.2.7. Analysis of Signals

With the microcontroller, there is only one time to trigger the TRIAC; however, this time is intrinsically linked to the firing angle. Knowing that the largest possible firing angle is 360° (2π) and the time (ms) for this firing is 16.67ms (60Hz), then the relationship between these parameters is time (ms) = $0.0463\alpha(\circ)$.

Therefore, a time of approximately 0.5 ms is observed for each first step. Hence, this was the time chosen for the microcontroller's TIMER interruption. Therefore, the relationship between the firing angle of the TRIAC and the RMS voltage delivered to the load was analyzed. As it is a resistive load, there is no lag between current and voltage, so both can be analyzed under the same point. The concept of the effective value of a sinusoidal voltage or alternating current is directly linked to the power transferred by this pair of quantities; it is through the RMS value that the power associated with AC quantities can be compared with powers associated with DC quantities.

Mathematically, the effective value X_{ef} of a periodic quantity $x(t)$ s determined through the:

$$X_{ef} = \sqrt{\frac{1}{T} \int_0^T (x(t))^2 dt} \quad (2)$$

Given that the voltage varies with time in a sinusoidal fashion and that the triggering of the TRIAC causes a delay in the conduction, we have that:

$$v(t) = V_{max} \sin(\omega t) \quad (3)$$

$$V_{ef} = \sqrt{\frac{1}{(2\pi - \alpha)} \int_{\alpha}^{2\pi} (V_{max} \sin(\omega t))^2 dt} \quad (4)$$

Solving the equation X algebraically, we arrive at a relationship:

$$V = 127 \sqrt{1 - \alpha/2\pi + \sin(2\alpha)/4\pi} \quad (5)$$

As can be seen from Eq. 5, there is no linear fit. Thus, isolating α as a function of the RMS voltage was impossible. Thus, it was considered to use a numerical method to solve this equation.

Table 3. PID relationship with ZIEGLER-NICHOLS critical gain and period in a closed loop

Controller type	K_p	T_i	T_d
P	$0.5P_{cr}$	-	-
PI	$0.45 P_{cr}$	$1/12T_{cr}$	-
PID	$0.6 P_{cr}$	$0.5T_{cr}$	$0.125T_{cr}$

Using this procedure and the SISOTOOL tool, it was possible to obtain a value for the PID parameters that best controlled the process.

$$C = \frac{0.4(1 + 3400s)(1 + 86s)}{s} \quad (6)$$

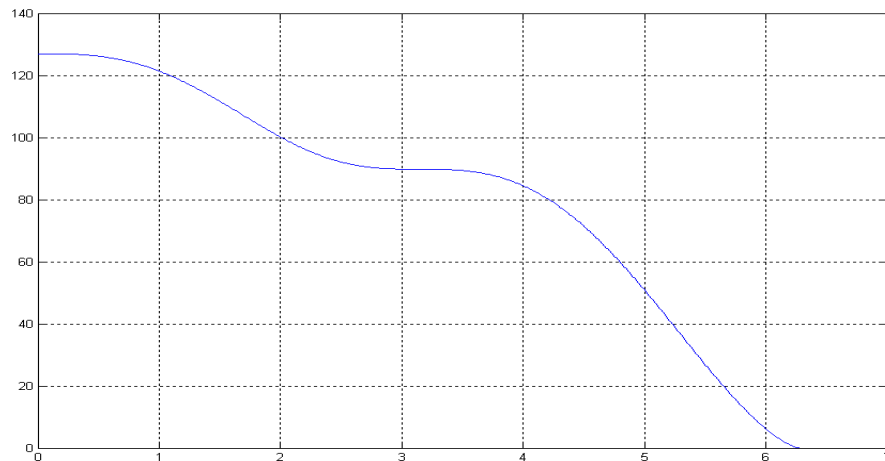


Fig. 14 RMS voltage as a function of firing angle (rad). It was noted that the relationship is not linear. For higher voltages, the firing angles are lesser and vice-versa. The curve starts from up to 120 V until 0 V when the firing angle reaches up to 6 rad

However, this would occupy the microcontroller, and thus it would not be possible to guarantee the sample rate predicted at the beginning of the calculations; this solution became unfeasible. Therefore, a table of values was used where the component looked for an angle value for a voltage range (lookup table), and this resulted in good results, both in terms of speed and program space. Therefore, controlling all input and output variables through C programming was possible.

4.2.8. Calculations of PID Parameters

To calculate the PID parameters, it was necessary to find the dynamics of the plant. Then, a mathematical model for the plant was approximated using the microcontroller itself and the MATLAB software. First, a program was made to acquire temperature values every 5 seconds. Then, three values of shooting angles were selected, 0°, 90° and 270°. Each angle arrived at an equilibrium temperature, however, showing similar dynamics as seen in the graph of Fig. 15.

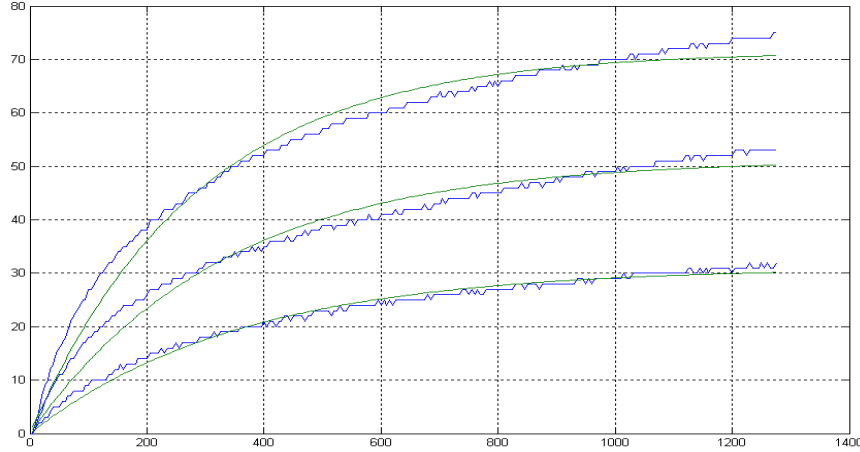


Fig. 15 Temperature-Environment Temperature (T-Tamb) as a function of time (tempo s) for the following firing angles 0, 90 and 270°. This test was carried out using a 100 W incandescent lamp inside a closed metal box. In green is shown the curve obtained by MATLAB (soft curve), and in blue is the curve obtained experimentally (rough curve)

The mathematical model used in MATLAB to fit the experimental data is represented by the equation:

$$T(t) = K \left(1 - e^{t/\tau} \right) \quad (7)$$

Therefore, MATLAB provided the following data for K and τ , considering the mean between the experimental curves.

$$T(t) = 0.50548 \left(1 - e^{t/323.67} \right) \quad (8)$$

Using this model for the plant, it was possible to use the SISOTool tool from MATLAB to adjust the PID parameters chosen in this process. However, to obtain an initial value for the PID, the closed-loop ZIEGLER – NICHOLS technique was applied. This method occurs when the closed loop system presents an oscillatory behavior with only a proportional controller. From this critical gain (Pcr) and the oscillation period (Tcr), a relatively good value can be found through Table 3.

$$C = \frac{0.4(1 + 3400s)(1 + 86s)}{s} \quad (9)$$

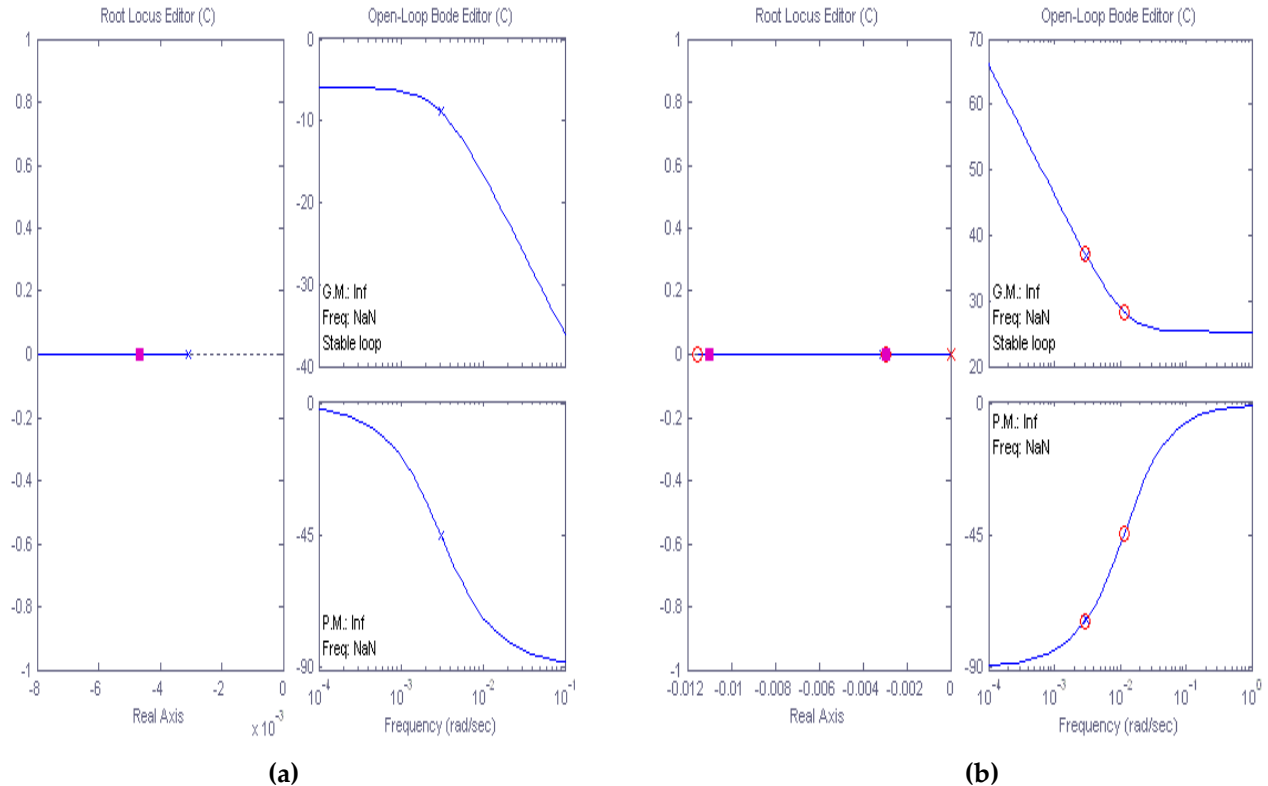


Fig. 16 Geometric locus of roots and the Bode diagram are both used to determine the most suitable PID values. These values were used because they resulted in a shorter rise time than the plant without the controller and because they left the system overdamped (poles on the real axis) (a) System without compensation and (b) with compensation.

Therefore, the system's typical response to a step change in temperature is shown in Fig. 17. A rapid growth until a bit less than 500 s, and then stops sloping after 500 s.

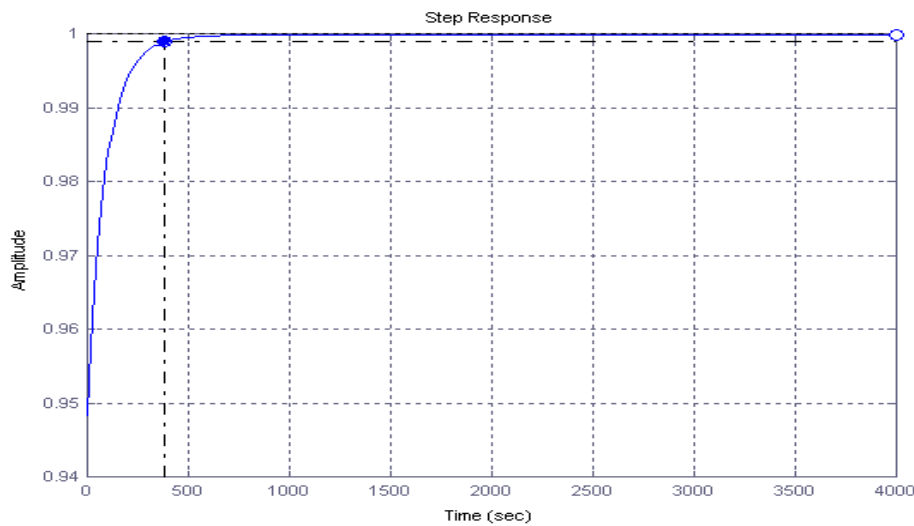


Fig. 17 PID response for one temperature step response of the compensated system. The graphs were expressed with the amplitude as a function of time

It can be seen that the system was overdamped, so there was no overshoot, which can not be very suitable in vacuum systems since radiation is the only way for the system to lose thermal energy.

4.2.9. Preliminary Control Tests

Using a 100 W tungsten incandescent lamp as a load, the results table was set up for three different temperatures, where both the rise time and the measurement error can be analyzed. Table 4 describes the data obtained in this preliminary testing stage. Both the times and the temperatures measured were analyzed from the microcontroller's memory, which acquires signals every 5 seconds. The temperature considered stationary was the one that proved to be continuous in 10 consecutive samples.

Table 4. Results obtained for the temperature control of the lamp placed inside a closed metallic box.

Expected temperature	Resulting temperature	Ascent time
30 °C	27.7 °C	8.0 min.
60 °C	55.1 °C	7.5 min.
90 °C	94.8 °C	7.3 min.

The results found indicate a difference of 5% in the temperature values. However, this difference may be reduced by adjusting the PID parameters and increasing the voltage data table by the TRIAC firing angle. In addition, it is suggested to repeat the procedure for the thermal plant consisting of a microtubular electrical resistance inside the vacuum chamber during the thin film growing in a low-pressure atmosphere. Moreover, Fig. 18 shows the frontal photo of the Power Controller with hot filament, while his caption shows the procedure to use the product.

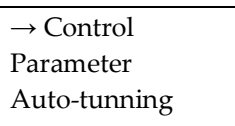


Fig. 21 Photo of the case of the power controller with hot filament

Procedure to use (set up) the power controller is given respectively in seven sequent steps:

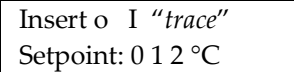
1° - On/off button to turn on the power controller.

2° - Menu:



The A button moves the arrow between the three menu options. With the arrow pointing to the "control" option, press the C (Enter) button.

3° - Insert the setpoint (Desired temperature)



The parameter "trace" indicates which temperature unit will be changed, and button B moves this dash over the unit, tens or hundreds of the temperature. To enter the value of the setpoint, move the trace over the unit by pressing button B. When the trace is over the unit, press button A, whose function is to increment by one the value that is below the trace. Once the unit value has been entered, press button B again, which will move the trace over the ten of the setpoint, in which pressing button A will increase this value. Finally, again, by pressing button B, the trace will be shifted to the hundredth of the setpoint, and by pressing button A, the temperature will be increased to the desired value.

4° - After inserting the desired setpoint, press "C" – ENTER.

5° - The Kp, Ki, and Kd parameters will appear, which will be used and do not need to be changed. So again, press the C –ENTER button, and the control will be initialized.

6° For "RESET" the process, after the start of the control, press button C again.

7° Turn off the temperature controller on the on/off button on top of the case.

5. Conclusion

This work revealed the effectiveness of a control widely used recently, the PID control. This type of approach for different types of plants may be implemented in different ways. However, with the evolution of digital devices, several researchers and products use programmable components to perform PID control.

5.1. Principal Conclusion

In this work, it was showed the effectiveness of a currently used control, the PID control. This type of approach for different types of plants may be implemented in different ways. On the other hand, with the evolution of digital devices, several researchers and products use programmable components to perform PID control. The parameter Temperature investigated was accomplished and useful for oxide thin film growth.

Authors' contributions

The authors contributed to drafting, interpreting data, preparing the paper, and editing and finalizing the manuscript. All authors approved the version of the manuscript to be submitted.

Acknowledgement and Funding

This review paper has been supported by the Brazilian agencies: PIBIC, CNPq and FAPESP. In addition, This study was financed in part by the Coordenação de Aperfeiçoamento de Pessoal de Nível Superior – Brasil (CAPES) – Finance Code 001.

References

- [1] Issues in Nanotechnology, Science, vol. 290, p. 1523, 2000.
- [2] T. Ando et al., *Mesoscopic Physics and Electronics*, Springer-Verlag, Germany, 1998. [[CrossRef](#)] [[Google Scholar](#)] [[Publisher Link](#)]
- [3] Edward L. Wolf, *Nanophysics and Nanotechnology: An Introduction to Modern Concepts in Nanoscience*, John Wiley & Sons, 2004. [[CrossRef](#)] [[Google Scholar](#)] [[Publisher Link](#)]
- [4] Vitaliy A. Shchukin, and Dieter Bimberg, "Spontaneous Ordering of Nanostructures on Crystal Surfaces," *Review of Modern Physics*, no. 71, pp. 1125, 1999. [[CrossRef](#)] [[Google Scholar](#)] [[Publisher Link](#)]
- [5] Dieter Bimberg, Marius Grundmann, and Nikolai N. Ledentsov, *Quantum Dot Heterostructures*, John Wiley & Sons Ltd., 1999. [[Google Scholar](#)] [[Publisher Link](#)]
- [6] Pierre Petroff, Axel Lorke, and Atac Imamoglu, "Epitaxially Self-Assembled Quantum Dots," *Physics Today*, no. 46, 2001. [[CrossRef](#)] [[Google Scholar](#)] [[Publisher Link](#)]
- [7] Vladimir V. Tsukruk et al., *Advances in Scanning Probe Microscopy of Polymers*, Wiley-VCH, 2001. [[Publisher Link](#)]
- [8] J. Chen et al., "Photovoltaic Devices Based on Poly(Bis-Terthiophenes) and Substituted Poly," *Synthetic Metals*, vol. 137, pp. 1373-1374, 2003. [[CrossRef](#)] [[Google Scholar](#)] [[Publisher Link](#)]
- [9] Karin Potje-Kamloth, "Chemical Gas Sensors Based on Organic Semiconductor Polypyrrole," *Critical Reviews in Analytical Chemistry*, vol. 32, no. 2, pp. 121-140, 2002. [[CrossRef](#)] [[Google Scholar](#)] [[Publisher Link](#)]
- [10] H K Yasuda, *Plasma Polymerization*, Academic Press Inc., Orlando, 1985. [[Google Scholar](#)] [[Publisher Link](#)]
- [11] Nicholas Morosoff, "An Introduction to Plasma Polymerization," *Plasma Deposition, Treatment and Etching of Polymers*, Academic Press Inc, New York, pp. 1-3, 1990. [[CrossRef](#)] [[Publisher Link](#)]
- [12] Shinzo Morita, and Shuzo Hattori, "Applications of Plasma Polymers," *Plasma Deposition, Treatment and Etching of Polymers*, Academic Press Inc, New York, pp. 423-461, 1990. [[CrossRef](#)] [[Google Scholar](#)] [[Publisher Link](#)]
- [13] Frank F. Shi, "Recent Advances in Polymer Thin Films Prepared by Plasma Polymerization Synthesis, Structural Characterization, Properties and Applications," *Surface and Coatings Technology*, vol. 82, no. 1, pp. 1-15, 1996. [[CrossRef](#)] [[Google Scholar](#)] [[Publisher Link](#)]
- [14] H. Biederman, and Y. Osada, "Plasma Polymerization Processes," Elsevier, Amsterdam, 1992.
- [15] J. M. Tibbitt, M. Shen, and A. T. Bell, "Structural Characterization of Plasma-Polymerized Hydrocarbons," *Journal of Macromolecular Science: Part A - Chemistry*, vol. 10, pp. 1623, 1976. [[CrossRef](#)] [[Google Scholar](#)] [[Publisher Link](#)]
- [16] F. L. Freire Jr., "Amorphous Hydrogenated Carbon Films: Effects Of Nitrogen And Fluorine Incorporation On The Film Microstructure And Mechanical Properties: A Review," *Journal of Non-Crystalline Solids*, vol. 304, no. 1-3, pp. 251258, 2002. [[CrossRef](#)] [[Google Scholar](#)] [[Publisher Link](#)]
- [17] Jung H. Lee et al., "Mechanical properties of a-C:H and a-C:H/SiO_x nanocomposite thin films prepared by ion-assisted plasma-enhanced chemical vapor deposition," *Thin Solid Films*, vol. 280, pp. 204-210, 1996. [[CrossRef](#)] [[Google Scholar](#)] [[Publisher Link](#)]
- [18] Edwin C. Lowenberg, *Electronic Circuits*, McGraw-Hill do Brasil, 1974. [[Google Scholar](#)] [[Publisher Link](#)]
- [19] A. Ahmed, *Power Electronics*, 1st ed., São Paulo: Prentice Hall, 2000. [[Google Scholar](#)] [[Publisher Link](#)]
- [20] A. P. Malvino, *Electronics – Vol. 1* (Translation: José Lucimar do Nascimento; technical proofreader: Antonio Pertence Junior), 4th ed., São Paulo - Brasil: Makron Books, 1995.
- [21] S. Schlüter et al., "Pore-Scale Displacement Mechanisms as a Source of Hysteresis for Two-Phase Flow in Porous Media," *Water Resources Research*, vol. 52, no. 3, pp. 2194, 2016. [[CrossRef](#)] [[Google Scholar](#)] [[Publisher Link](#)]
- [22] K. Ogata, *Modern Control Engineering*, Prentice-Hall. [[Google Scholar](#)]
- [23] A. L. Barabasi, and H. E. Stanley, *Fractal Concepts in Surface Growth*, Cambridge University Press, Cambridge, p. 19-28, 1995. [[CrossRef](#)] [[Google Scholar](#)] [[Publisher Link](#)]
- [24] Milton Ohring, *The Materials Science of Thin Films*, 1 ed., Academic Press. San Diego, p. 794, 1992. [[Google Scholar](#)] [[Publisher Link](#)]
- [25] Mehran Kardar, "Dynamic Scaling Phenomena in Growth Processes," *Physica B: Condensed Matter*, vol. 221, pp. 60-64, 1996. [[CrossRef](#)] [[Google Scholar](#)] [[Publisher Link](#)]